Volume 1 | Number 1 | Jan 2013 | Pages 1–100

Journal of
Materials Chemistry A

Materials for energy and sustainability
www.rsc.org/materialsA

ROYAL SOCIETY
OF CHEMISTRY

ROYAL SOCIETY
OF CHEMISTRY

www.rsc.org/materialsA

Pristine-state structure of lithium-ion-battery cathode material Li1.2Mn0.4Co0.4O2 derived from NMR bond pathway analysis

Hakim Iddir[1], Baris Key[2], Fulya Dogan[2], John T. Russell[1], Brandon R. Long[2], Javier Bareño[2], Jason R. Croy[2] and Roy Benedek[2]

[1] Materials Science Division, Argonne National Laboratory, Argonne, IL 60439

[2] Chemical Sciences and Engineering Division, Argonne National Laboratory, Argonne, IL 60439

ABSTRACT: Layered lithium ion battery cathode materials have been extensively investigated, of which layered-layered composites xLi$_2$MnO$_3$•($1-x$)LiMO_2 (M=Mn,Co,Ni) are of particular interest, owing to their high energy density. Before the structural transformations that occur in these materials with cycling can be understood, the structure of the pristine material must be established. In this work, NMR spectra are measured for the model layered-layered system xLi$_2$MnO$_3$•($1-x$)LiCoO$_2$ and Bond-Pathway-model analysis is applied to elucidate the atomic arrangement and domain structure of this material in its pristine state, before electrochemical cycling. The simplest structural element of an Li$_2$MnO$_3$ domain consists of a stripe of composition LiMn$_2$ parallel to a crystallographic axis in a metal layer of the composite. A simple model of the composite structure may be constructed by a superposition of such stripes in an LiCoO$_2$ background. We show that such a model can account for most of the features of the observed NMR spectra.

I. Introduction

Layered-layered composite cathode materials for lithium ion batteries[1] with composition xLi$_2$MnO$_3$•($1-x$)LiMO_2 have attracted enormous attention because of their high capacities and energy densities. Because microstructural features are expected to influence battery performance, a better characterization of the material structure and transformations would be valuable. Experimental observation[2] shows evidence of fine scale phase separation into Li- and Mn-rich domains and transition metal (TM)-rich domains (Long et al 2014). TEM[2] indicates that the Li- and Mn-rich domains exhibit the ordering of the LiMn$_2$ layers characteristic of pure Li$_2$MnO$_3$. Furthermore, modeling[3] suggests that the solubility of Li$_2$MnO$_3$ in LiMO_2 is negligible, which implies that phase separation would occur at thermodynamic equilibrium.

Although these features are reasonably well established, they fall short of a detailed characterization of the atomic structure. Uncertainty remains, for example, as to the shape and size of the domains, both of which are likely dependent on composition and synthesis procedures. Without a better understanding of the atomic arrangement of the pristine materials, it is unlikely that a realistic picture of the transformations that occur upon cycling can be developed. Atomistic simulation methods, for example density functional theory or molecular dynamics, require a starting structure from which to proceed. De-

spite the enormous literature on layered-layered composites, the understanding of the cycling-driven transformations is scant. This article is intended as a step towards determining a realistic starting structure.

NMR spectroscopy based on the Magic-Angle-Spinning (MAS) technique is an attractive probe of the structural features of complex materials such as transition-metal oxides[4]. In many paramagnetic lithium-ion battery materials, measured NMR frequency shifts are dominated by the Fermi-contact interaction[5], which is sensitive to atomic arrangements on a sub-nanometer scale. NMR is particularly suited to characterize materials with substitutional disorder such as xLi$_2$MnO$_3$•($1-x$)LiMO_2 composites. Local lithium environments within domain interiors, or at domain boundaries, are expected to exhibit unique signatures, i.e. resonance frequencies, in the NMR spectrum. The observed spectrum is given by a linear superposition of the contributions of each observed center Li. The superposition of intensities, in NMR, rather than amplitudes, as in X-ray diffraction, greatly simplifies the analysis.

The standard composition Li$_{1.2}$Mn$_{0.4}$Co$_{0.4}$O$_2$, a composite with equal parts Li$_2$MnO$_3$ and LiCoO$_2$ was selected for this work. It is shown below that NMR spectra of Li$_{1.2}$Mn$_{0.4}$Co$_{0.4}$O$_2$ powders exhibit low-frequency features that result exclusively from lithium at domain boundaries. These features provide helpful guidance for our do-

main modeling. The different coordination environments of lithium ions (number of Co and Mn neighbors) result in well-resolved NMR shifts.

Since the local atomic arrangements responsible for individual observed NMR spectral features are not known *a priori*, modeling is required to help identify them. First-principles density functional theory[6] provides a rigorous approach. The prediction of characteristic frequencies based on first principles calculations of hyperfine parameters[6] is not always feasible, however, particularly for highly disordered systems with unknown short-range atomic order. A simpler approach is to apply the Bond-Pathway analysis method[5] to atomic arrangements identified, for example, from DFT calculations, as described below. More approximate than first principles calculation of hyperfine parameters, the Bond-Pathway analysis method employs empirical parameters, which enable frequency shifts to be readily predicted for a given atomic arrangement. In this work, we apply the Bond-Pathway analysis method to help characterize the domain structure in the model composite system based on *M*=Co.

II. Experimental

Lithium-6 enriched $Li_{1.2}Mn_{0.4}Co_{0.4}O_2$ was prepared as in previous work[7]. An oxalate $Mn_{0.5}Co_{0.5}C_2O_4$ precursor was thoroughly mixed with a stoichiometric amount of lithium-6 enriched lithium carbonate (Cambridge Isotopes) and pre-heat treated at 550°C (~2°C/min ramp) for 12 hours in air. This baseline material was then used in three separate firing experiments for different amounts of time in air as detailed below.

High-resolution ($\Delta Q/Q \approx 2 \times 10^{-4}$) synchrotron X-ray powder diffraction data (HR-XRD) were collected using beamline 11-BM at the Advanced Photon Source (APS), Argonne National Laboratory. Scans were collected in transmission mode on spinning Kapton capillaries using a fixed wavelength of 0.413753 Å. 2θ values are reported on the CuKα scale for ease.

High-resolution X-ray diffraction patterns for the as-prepared [6]Li enriched $Li_{1.2}Mn_{0.4}Co_{0.4}O_2$ powders, with increasing annealing time, are shown in figure 1. The patterns are typical of layered-layered composite materials with the main diffraction peaks indexed to rhombohedral $R\bar{3}m$ symmetry. The so-called superstructure peaks between ~20-32° 2θ (Fig. 1 inset), which cannot be indexed to $R\bar{3}m$, indicate Li-TM ordering ($LiMn_6$ complexes) with monoclinic C2/m symmetry. The peak broadening is influenced by stacking defects in the *c*-axis direction of the Li_2MnO_3 regions[2, 8], and therefore does not provide direct information about domain structure. Stacking defect densities diminish with increased annealing times, which results in sharper and more intense diffraction peaks. The decrease in stacking defects with annealing time, revealed by HR-XRD, is also reflected in enhanced intensity of features related to specific Li environments in the NMR spectra.

[6]Li MAS-NMR measurements were made at fields of 7.02 Tesla (300 MHz) on a Bruker Avance III HD spectrometer operated at a Larmor frequency of 44.21 MHz, using a 1.3 mm MAS probe. Spectra were acquired at 67 kHz spinning speed with a rotor synchronized echo pulse sequence (90°-τ-180°-τ-acquisition), where τ= 1/v_r. A π/2 pulse width of 1.5 μs was used with sufficiently long pulse recycle time delays of 0.2 s [9]. Data were collected at a constant temperature of 283 ± 0.1 K to avoid any effects of chemical shift temperature dependence. Chemical shifts were referenced to 1M LiCl at 0 ppm.

III. Density Functional Theory Calculations

First principles calculations were performed with the VASP code[10], in the PAW representation[11], with the PBE exchange-correlation potential[12], at the GGA+*U* level[13]. Effective Hubbard constants *U*=4.0 eV for Mn and 5.0 eV for Co were used. Most calculations employed a single k-point.

The composition employed in DFT calculations is $Li_{7/6}Mn_{1/3}Co_{1/2}O_2$, close to the standard composition $Li_{1.2}Mn_{0.4}Co_{0.4}O_2$ on which the presented measurements were performed. The computational supercell was based on 96 formula units (384 atoms).

For each candidate domain configuration, the atomic coordinates were optimized to minimize the energy, and determine relaxed local atomic configurations. The candidate domain configurations are discussed in the following section. The resultant relaxed atomic structure is then used as input to the Bond Pathway model analysis to predict the corresponding NMR spectra.

IV. Simulation of NMR Spectra

A. Bond Pathway model

The Bond-Pathway model analysis method is a phenomenological formulation of the Fermi-contact interaction frequency shifts associated with spin density at an observed (Li ion) center, *i*. The frequency shift results from the proximity of R_i to transition metal ions with non-zero spin density, each of which induces a paramagnetic spin on the observed center through a molecular orbital that traverses an Li-O-M trimer (pathway). The net frequency shift is expressed as a sum of contributions from such trimers:

$$\omega_i = \sum_{j,k} g(r_{ij}, r_{kj}, \theta_{ijk}), \tag{1}$$

where $r_{ij} = R_i - R_j$, R_i represents the location of an observed (Li ion) center, R_j is the location of a near-neighbor oxygen ion, and R_k is the location of an Mn ion,

and θ_{ijk} is the angle between r_{ij} and r_{kj}. The full NMR spectrum is then given by the superposition

$$A(\omega) = \sum_i \delta(\omega - \omega_i) \qquad (2)$$

of contributions from individual Li ions. The expression of A in terms of delta functions in Eq.(2) is an idealization that neglects the broadening in a real measurement. Spectral broadening may occur, e.g., as a result of lattice defects, thermal vibrations, and the incomplete suppression of anisotropy by magic-angle spinning. In numerical calculations, the delta function is replaced by a suitable broadening function; Gaussian broadening was used in the present work.

The utility of Eq. (1) hinges on the availability of a simple but accurate approximation for $g(r,r',\theta)$. For the layered-layered composite compounds of interest in the present work, the nearest neighbor ijk trimers have an included angle close to either 90 or 180 degrees, apart from lattice distortion. The two-parameter representation

$$g = g_1: \quad \theta_{ijk} \approx \pi/2,$$
$$\quad\; g_2: \quad \theta_{ijk} \approx \pi, \qquad (3)$$

was found to give an excellent description of layered metal oxides with $R\bar{3}m$ (or $C2/m$) symmetry; parameterizations for other metal oxides were also given[4]. The values g_1=125, and g_2=-60, in ppm are employed in the present work. Slightly different values of g_1 and g_2 give essentially the same level of agreement with experiment. The measured peak positions may also vary by of order 1% from one specimen to another.

The Li ions in the Li layer of Li_2MnO_3 occupy both 2c and 4h Wyckoff positions. In both cases, Li connects to Mn through 12 Li-O-Mn pathways, 8 with angle 90 degrees and 4 with 180 degrees, so that

$$\omega(Li_{2c}) \;[\text{or}\; \omega(Li_{4h})] = 8g_1 + 4g_2 = 760 \text{ ppm.} \qquad (4)$$

The Li ions in the Mn layer occupy 2b sites, which have 12 90-degree Li-O-Mn pathways, so that

$$\omega(Li_{2b}) = 12\,g_1 = 1500 \text{ ppm.} \qquad (5)$$

The parameters g_1 and g_1 were selected to closely reproduce the measured frequency shifts $\omega(Li_{2c})$ and $\omega(Li_{2b})$ [4].

Since Eq.(3) is empirical, no systematic correction procedure to the lowest-level approximation is presently available. For a composite material, however, it would be desirable to account in some way for the disorder in bond lengths and bond angles. In Eq.(7) below, we suggest a heuristic interpolation scheme for the θ dependence of $g(r,r',\theta)$.

B. Frequency regimes

In this work, we apply the Bond-Pathway model to xLi$_2$MnO$_3$•(1-x)LiCoO$_2$, to elucidate its domain structure. For this system, only Li-O-Mn pathways contribute, since Co adopts a non-magnetic trivalent state (cf. last paragraph in section C, however) (Bareno and Long et al 2014). For other layered-layered composites, for example those based on M=Mn$_{0.5}$Ni$_{0.5}$, a separate parameter g_{Ni}, as well as g_{Mn}, is required. Although a numerical value for g_{Ni} is available[4], the additional complication in Ni-bearing materials is significant. Analysis of composite materials that include Mn and Ni will be presented elsewhere.

According to Eq.(3), the frequency shifts in the MnCo system can be expressed as

$$\omega_i = N_1(i)\, g_1 + N_2(i)\, g_2, \qquad (6)$$

where $N_t = N_1 + N_2 \leq 12$. Thus, each Li ion is bonded to six O ions, which each have two Mn nearest neighbors. In the interior of the domains, $N_t = 12$, however, at the interface between the Li$_2$MnO$_3$ domains and the LiCoO$_2$ regions, fewer trimers contribute to ω_i. Typically, frequencies for Li near domain interfaces are smaller than those corresponding to N_t =12 [cf. Eqs. (4) and (5)]. We note that Eq.(6) may yield negative frequencies for some combinations of N_1 and N_2, in view of the negative value of g_2. The spectra in Fig.2 do show nonzero intensity at negative frequency shifts.

To account for deviations of θ_{ijk} from their ideal values of $\pi/2$ and π (Eq.(3)) in the xLi$_2$MnO$_3$•(1-x)LiCoO$_2$ composite, we apply the linear interpolation,

$$\omega_i(\theta_{ijk}) = \sum_{j,k} \frac{2}{\pi}(g_2 - g_1)\theta_{ijk} + 2g_1 - g_2. \qquad (7)$$

Equation (7) is no doubt oversimplified, but appears adequate for our present purposes. Using this method, a spectrum is calculated for atomic arrangements obtained from DFT calculations, as described below. Each observed Li center contributes a shift, ω_i, which is tabulated in a histogram with a bin width of 10 ppm. We apply a Gaussian broadening (20 ppm) to the histogram to simulate a NMR spectrum for comparison with experiment.

As described in section II, spectra for the layered composites Li$_{1.2}$Mn$_{0.4}$Co$_{0.4}$O$_2$ that correspond to specimens prepared with different annealing times (at 850 deg. C) are plotted in Fig. 2. The spectra show peaks consistent with the frequencies given in Eq. (4) and (5) for bulk Li$_2$MnO$_3$. We attribute the spectra at frequencies lower than $\omega_1 \approx 500$ ppm to Li at domain interfaces; within the bond-pathway model, only domain-interface Li ions have environments with (N_1, N_2) values consistent with these lower frequencies.

Two general aspects of the domain interfaces may be inferred without detailed calculation. First, the sharp features observed in the NMR spectrum at $\omega < \omega_1$ suggest

3

that a high density of characteristic domain interface structures must be present; if the interfaces were more random, with nondescript structures, a more broadened NMR spectrum would be expected, in contrast to the blue curve in Fig. 2. Furthermore, the density of Li ions located at domain interfaces must be appreciable, to account for the large integrated intensity of the spectra for frequency shifts below ω_1. These observations help constrain the candidate structural models considered below.

C. Domain Structure

As mentioned earlier, the atomic structure of the pristine material $x\mathrm{Li_2MnO_3}\cdot(1-x)\mathrm{LiCoO_2}$ appears to be a composite of $\mathrm{LiMn_2}$ patches (similar to those in $\mathrm{Li_2MnO_3}$) embedded in a Co-rich background. We refer to such an arrangement as a domain structure. The objective of this work is to characterize the domain structure in more detail. Our approach was guided by the following assumptions, which are suggested by the form of the Bond-Pathway analysis model, Eqs. (1-7). First, if line broadening (treated via Eq. (7) in the present work) is neglected, resonance frequencies are uniquely determined by the number of 90 degree and 180 degree trimers (N_1 and N_2) of Observed Li Centers i: $\omega_i = \omega_i (N_1, N_2)$ [cf. Eq. 6)]. Therefore, apart from line broadening, the Bond-Pathway model predicts only a relatively small number of discrete resonance frequencies, since N_1 and N_2 take on only a few values for the given crystal lattice. Within this picture, it remains only to specify how often particular trimer environments (N_1, N_2) occur in the actual domain structure, which determines the relative intensities of the resonance peaks. A further assumption is that the domain structure (or admixture of structures) for which the predicted NMR spectrum matches the measured one is essentially unique; spurious atomic structures whose bond-pathway-model spectra "accidentally" reproduce the observed NMR spectrum are unlikely. These assumptions seem reasonable, although not strictly provable.

We focus in the following on a class of non-compact domain structures. The simplest such high aspect ratio domain is a stripe (or ribbon) with composition $\mathrm{LiMn_2}$ aligned parallel to one of the main in-plane crystallographic axes, e.g., $[11\bar{2}0]$ or $[1\bar{1}00]$. (Non-compact domains have been observed in TEM[8].) Such ribbons represent the two lowest-index orientations of the $\mathrm{LiMn_2}$/Co interface. A stripe with orientation $[11\bar{2}0]$ is illustrated in Fig. 3. Three-dimensional domains may be thought of as the stacking the stripes in successive (metal) layers along the c-axis.

Our analysis is restricted to domains built from striped structural elements. We exclude from consideration more compact (lower aspect ratio) domains, since, as noted in section B, domains in which a wide variety of Li-ion-site environments [different (N_1, N_2)] occur appear inconsistent with the small number and sharpness of the low frequency (less than 500 ppm) spectral features seen in Fig. 2. Thus, the uniformity of Li ion environments possessed by striped or ribbon domains, appears to be required to reproduce the measured spectra.

If stripes represent the dominant structural element, then the full structure of the composite pristine material can essentially be represented by arrays of striped domains. For simplicity, we consider structures that comprise periodic arrays of striped domains. A more general set of composite structures could include the possibility of point defects (such as antisite disorder) in the domains; an example is given below. Although this family of composite structures is a small subset of the phase space of possible structures with the given composition, we find that it already is able to account for most of the significant features in the measured spectra shown in Fig. 2.

Apart from the orientation of the stripes, two other degrees of freedom of domains are the stripe thickness and the in-layer offset of stripes in adjacent layers. The thickness of the ribbon (in an LMC layer) is proportional to the number of $\mathrm{LiMn_2}$ rows in each stripe; the stripe in Fig.3, for example, is 4 rows thick. The experimental spectrum in Fig. 2 constrains the stripe to be not too thin or too thick; for a very thin domain, the bulk frequencies, above $\omega > \omega_1$, would disappear; a thick stripe, however, would diminish the lower frequency spectral intensities for $\omega < \omega_1$ too much to be in accord with experiment.

The "offset" refers to how the ribbons are stacked along the c-axis. According to DFT calculations, a minimal offset is energetically preferred, as well as a ribbon orientation parallel to an in-plane crystallographic axis. Thus, low-index $[11\bar{2}0]$ or $[1\bar{1}00]$ facets are preferred as the bounding surfaces of $\mathrm{Li_2MnO_3}$ domains.

Figure 4 shows predicted NMR spectra for different choices of the offset and ribbon orientation (un-rotated or rotated by 30 degrees, relative to an in-layer crystallographic axis) degrees of freedom. The label "No offset" indicates that the distance between equivalent atoms in adjacent ribbons is the smallest possible consistent with the crystal structure, which results in a low index interface between the $\mathrm{Li_2MnO_3}$ and $\mathrm{LiCoO_2}$ domains. The label "Full offset" indicates that ribbons in adjacent $\mathrm{LiMn_2}$-Co layers are sufficiently shifted so that no overlap occurs in the vertical direction. "Partial offset" indicates an intermediate shift, depicted in Figure 5.

The lowest calculated energy corresponds to the (minimal offset, non-rotated) case. The corresponding spectrum (black curve in Fig. 4) reproduces some of the features of the measurement in the regime $\omega < \omega_1$, in particular, peaks at about 400 ppm. Nevertheless, there is a significant shoulder at frequency higher than 400 that does not appear in this simulation. Moreover, in the simulated spectra, the intensities of the shifts characteristic of $\mathrm{Li_2MnO_3}$ domains, are higher than the intensity of the shifts originating from the interface boundaries.

Fully offset (i.e., isolated) $\mathrm{LiMn_2}$ stripes, for which a LL Li interacts with only a single stripe, would not exhibit bulk $\mathrm{Li_2MnO_3}$ NMR signatures. Partially offset stripes, however, can satisfy both requirements, namely, low intensity of $\mathrm{Li_2MnO_3}$ peaks, provided by the $\mathrm{LiMn_2}$-$\mathrm{LiMn_2}$

overlap domains, and relatively higher interface contributions to the overall NMR spectrum (see figure 5). The interface contributions are of two types for both Li in the Li layer (LL) and Li in the transition metal layer (TM): Li atoms near $LiMn_2$-Co interface (locations 2 and 4 in figure 5), and Li atoms in the LL, but sandwiched between $LiMn_2$ and Co domains on each side (location 5 in figure 5). Because of the additivity of frequency shifts at each Li site, the shift of Li in the LL near the interface (location 4), away from the $LiMn_2$-$LiMn_2$ overlap region (location 3) is approximately 1/4 of the typical bulk Li_2MnO_3 shift (i.e. ~760/4 = 190 ppm), whereas that of Li in the LL away from the interface and the overlap region (location 5) is about 760/2 = 380 ppm. Similarly, the Li shift in the TM near the interface (location 2) is about ½ of the TM signature (i.e. 1500/2 = 750 ppm). Locations 1 and 3 in figure 5 are shifts by Li_2MnO_3 bulk-like contributions.

Further inspection of the experimental NMR spectra, particularly the spectrum of the sample annealed for seven days (Fig. 2), shows that the intensity of the peak near 1000 ppm has drastically diminished. Our simulations indicate that such shifts originate from Li in the TM layer at the interface of the ribbon, coordinated to four Mn and two Co atoms. We find that a rotated stripe better reproduces this feature. Li at the interface of the TM layer has now only three Mn and three Li neighbors (Fig. 6), hence contributing to the 750 ppm shift, instead of the 2/3*(1500)=1000 ppm shift.

Actual three-dimensional domain shapes in real layered-layered LMR-NMC samples can be expected to be very complex, especially given the small differences in calculated energies (less than 35 meV per $Li_{7/6}Mn_{1/3}Co_{1/2}O_2$ formula unit) between different ribbon configurations; i.e., domain facets.

A simulated NMR spectrum for the rotated partially offset ribbon structure is shown in Fig. 4 (green curve S2). The intensity of the peak near 400 ppm is still not as sharp as in the experimental spectra. A linear combination of partially and fully offset ribbons (orange curve in Fig 4) gives improved agreement with experiment, as shown in Fig. 7. The $\omega_i = -50$ ppm peaks are also reproduced by the model. These shifts originate from Li-O-Mn at 180° configurations of Li in the LL and near the domain boundary.

We note that the experimental NMR spectra (Fig. 2) for shorter annealing times show a small peak near 1100 ppm. We have observed such shifts for cases in which we have Li substituted by Mn in the LL (10 Li-O-Mn paths at 90° and 3 paths at 180°). Annealing the samples for longer times might have allowed Mn to migrate to the TM layer instead of staying trapped in the LL.

D. Possible evidence for paramagnetic Co

The origin of the observed peak splitting near 1460 ppm is uncertain. $LiMn_5Co$ rings in the TM layer, if present (in addition to the characteristic $LiMn_6$ rings of Li_2MnO_3) might be responsible. Bond-Pathway model analysis, assuming nonmagnetic Co[14], would yield a shift of 1220-1250 ppm, whereas the observed unassigned peak resonates at

1360 ppm. A possibly analogous feature has been observed for $LiMn_5Ni$ units in NiMn composites[15-17]. Application of these results to the Mn-Co system suggests a shift range of 1300-1330 ppm for $LiMn_5Co$ units and makes this assignment plausible for the peak splitting near 1460 ppm.

DFT calculations were performed to investigate whether Co can contribute to the NMR shift in $LiMn_5Co$ units. An example of a non-stoichiometric ribbon domain was obtained by substituting a pair of Co ions with Mn ions near the ribbon interface ($LiMn_3Co_3$ interface). The Co within the $LiMn_5Co$ unit can then be paramagnetic and hence contribute to the overall shift produced by such a configuration (the paramagnetic solution is only 8 meV/f.u. higher than the diamagnetic solution). In fact the integrated net spin density around Li in the $LiMn_5Co$ unit is similar to the spin density of Li in $LiMn_6$ unit (+0.006). Although qualitative [6], this suggests a contribution to the NMR shift associated with paramagnetic Co.

IV. Summary

NMR spectroscopy is a sensitive probe of local atomic structure in layered-layered composite cathode materials for lithium ion batteries. Using Bond-Pathway model analysis, we have compared predicted spectra for candidate atomic arrangements of $Li_{1.2}Mn_{0.4}Co_{0.4}O_2$ composites with measured results. We have considered domain structures that can be generated from $LiMn_2$ stripes along low index intra-layer crystallographic directions; more compact (lower aspect ratio) domains appear inconsistent with the measured spectra. We are able to reproduce the main features of the measured spectra with stripes only a few atomic rows thick and partially offset from those in adjacent layers. A combination of stripes along more than one crystallographic axis yields the best agreement with experiment.

AUTHOR INFORMATION

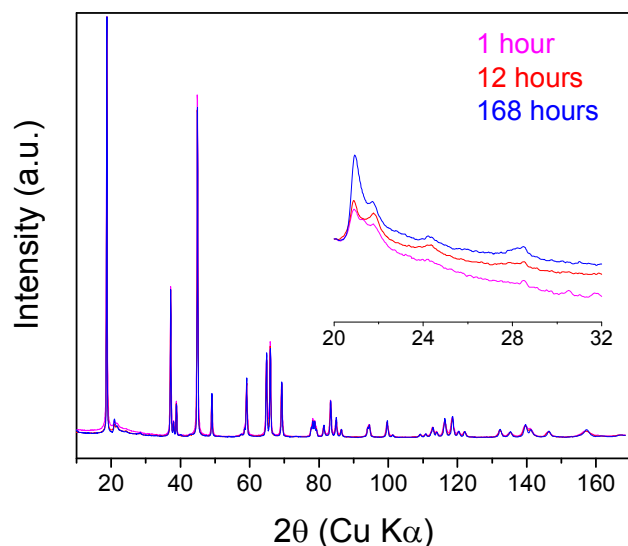**Corresponding Author**
iddir@anl.gov

Author Contributions
All authors contributed equally.

Fig. 1. Powder high-resolution X-ray diffraction patterns of the lithium-6 enriched $Li_{1.2}Mn_{0.4}Co_{0.4}O_2$ powders at different annealing times as indicated (lower: 1 h, middle: 12 h, and top: 168 h). Inset shows zoomed in region of Li_2MnO_3 superstructure peaks.
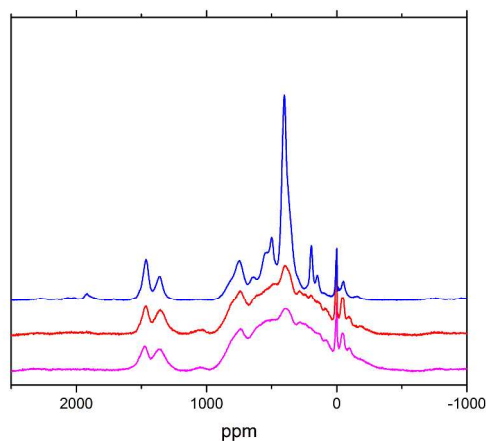

Fig. 2. Normalized NMR Spectra for $Li_{1.2}Mn_{0.4}Co_{0.4}O_2$. Results for three annealing times (Magenta [bottom]: 1hr at 850C/quenched, Red [middle]: 12hr at 850C regular cooled, Blue [top]: 168hr at 850C regular cooled) are shown.
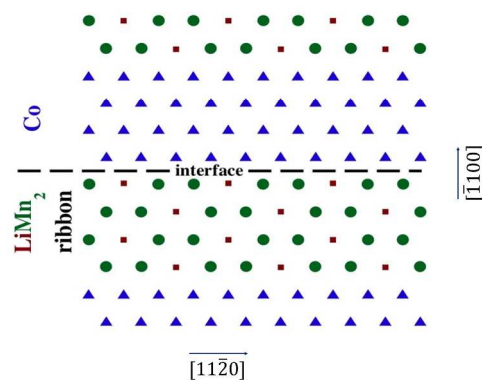

Fig. 3. Schematic illustration of (a single layer of a) ribbon domain in TM layer of xLi$_2$MnO$_3$•(1-x)LiMO_2 composite (M=Co).
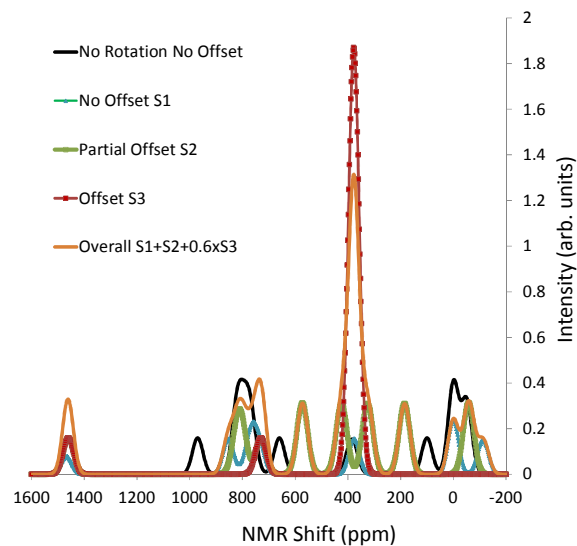

Fig. 4. Predicted NMR spectra for different domain configurations. "No offset" corresponds to LiMn$_2$ stripes stacked along the c-axis; "partial offset" and "offset" correspond to stripes in adjacent layers that are shifted by two or four atomic rows, respectively, relative to each other (stripes are four atomic rows thick [Fig.3]). Overall linear combination S1+S2+0.6S3 is the simulated NMR reported in fig. 7.
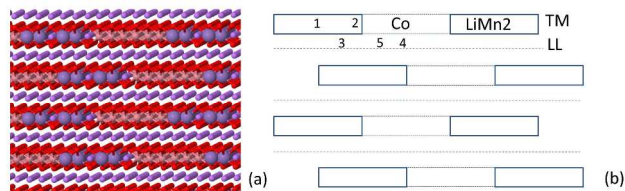
6

Fig. 5. (a) Ball and stick model of the ribbon structure partial stacking: O in red, Li in purple, Mn large atoms in gray, Co in orange. (b) Schematic of the same structure showing the different locations mentioned in the text.
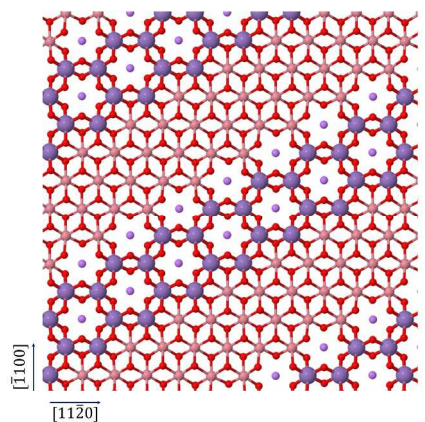

Fig. 6. Transition metal layer for the rotated domain. Atoms along atomic rows parallel to the domain are second neighbors.
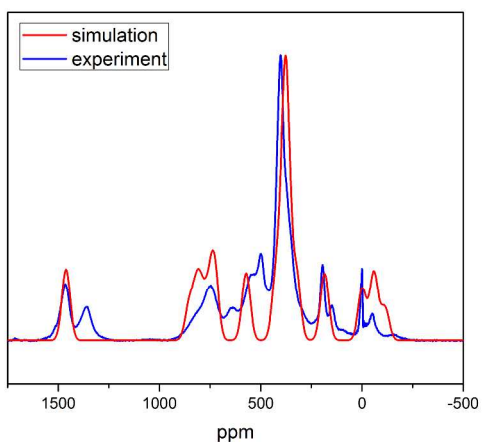

Fig. 7. Simulated spectrum and experimental NMR spectrum for $Li_{1.2}Mn_{0.4}Co_{0.4}O_2$ (annealed 168h).

REFERENCES

1.   Thackeray, M. M.; Kang, S.-H.; Johnson, C. S.; Vaughey, J. T.; Benedek, R.; Hackney, S. A., Li2mno3-Stabilized Limo2 (M = Mn, Ni, Co) Electrodes for Lithium-Ion Batteries. *Journal of Materials Chemistry* **2007**, *17*, 3112-3125.

2.   Boulineau, A.; Simonin, L.; Colin, J.-F.; Canévet, E.; Daniel, L.; Patoux, S., Evolutions of Li1.2mn0.61ni0.18mg0.01o2 During the Initial Charge/Discharge Cycle Studied by Advanced Electron Microscopy. *Chemistry of Materials* **2012**, *24*, 3558-3566.

3.   Iddir, H.; Benedek, R., First-Principles Analysis of Phase Stability in Layered–Layered Composite Cathodes for Lithium-Ion Batteries. *Chemistry of Materials* **2014**.

4.   Grey, C. P.; Dupre, N., Nmr Studies of Cathode Materials for Lithium-Ion Rechargeable Batteries. *Chemical Reviews* **2004**, *104*, 4493-4512.

5.   Middlemiss, D. S.; Ilott, A. J.; Clément, R. J.; Strobridge, F. C.; Grey, C. P., Density Functional Theory-Based Bond Pathway Decompositions of Hyperfine Shifts: Equipping Solid-State Nmr to Characterize Atomic Environments in Paramagnetic Materials. *Chemistry of Materials* **2013**, *25*, 1723-1734.

6.   Carlier, D.; Menetrier, M.; Grey, C. P.; Delmas, C.; Ceder, G., Understanding the Nmr Shifts in Paramagnetic Transition Metal Oxides Using Density Functional Theory Calculations. *Phys. Rev. B* **2003**, *67*, 174103.

7.   Long, B. R.; Croy, J. R.; Dogan, F.; Suchomel, M. R.; Key, B.; Wen, J.; Miller, D. J.; Thackeray, M. M.; Balasubramanian, M., Effect of Cooling Rates on Phase Separation in 0.5li2mno3·0.5licoo2 Electrode Materials for Li-Ion Batteries. *Chemistry of Materials* **2014**, *26*, 3565-3572.

8.   Bareño, J.; Balasubramanian, M.; Kang, S. H.; Wen, J. G.; Lei, C. H.; Pol, S. V.; Petrov, I.; Abraham, D. P., Long-Range and Local Structure in the Layered Oxide Li1.2co0.4mn0.4o2. *Chemistry of Materials* **2011**, *23*, 2039-2050.

9.   Meiboom, S.; Gill, D., Modified Spin-Echo Method for Measuring Nuclear Relaxation Times. *Review of Scientific Instruments* **1958**, *29*, 688-691.

10.   Kresse, G.; Furthmüller, J., Efficient Iterative Schemes for Ab Initio Total-Energy Calculations Using a Plane-Wave Basis Set. *Physical Review B* **1996**, *54*, 11169.

11.   Kresse, G.; Joubert, D., From Ultrasoft Pseudopotentials to the Projector Augmented-Wave Method. *Physical Review B* **1999**, *59*, 1758-1775.

12.   Perdew, J. P.; Burke, K.; Ernzerhof, M., Generalized Gradient Approximation Made Simple. *Physical Review Letters* **1996**, *77*, 3865.

13.   Dudarev, S. L.; Botton, G. A.; Savrasov, S. Y.; Humphreys, C. J.; Sutton, A. P., Electron-Energy-Loss Spectra and the Structural Stability of Nickel Oxide: An Lsda+U Study. *Phys. Rev. B* **1998**, *57*, 1505-1509.

14.   Zeng, D.; Cabana, J.; Breger, J.; Yoon, W.-S.; Grey, C. P., Cation Ordering in Li Nixmnxco(1-2x) O-2-Layered Cathode Materials: A Nuclear Magnetic Resonance (Nmr), Pair Distribution Function,

X-Ray Absorption Spectroscopy, and Electrochemical Study. *Chemistry of Materials* **2007**, *19*, 6277-6289.

15.   Breger, J.; Dupre, N.; Chupas, P. J.; Lee, P. L.; Proffen, T.; Parise, J. B.; Grey, C. P., Short- and Long-Range Order in the Positive Electrode Material, Li(Nimn)(0.5)O-2: A Joint X-Ray and Neutron Diffraction, Pair Distribution Function Analysis and Nmr Study. *Journal of the American Chemical Society* **2005**, *127*, 7529-7537.

16.   Yoon, W.-S.; Kim, N.; Yang, X.-Q.; McBreen, J.; Grey, C. P., 6li Mas Nmr and in Situ X-Ray Studies of Lithium Nickel Manganese Oxides. *Journal of Power Sources* **2003**, *119–121*, 649-653.

17.   Jiang, M.; Key, B.; Meng, Y. S.; Grey, C. P., Electrochemical and Structural Study of the Layered, "Li-Excess" Lithium-Ion Battery Electrode Material Li Li1/9ni1/3mn5/9 O-2. *Chemistry of Materials* **2009**, *21*, 2733-2745.